

## Article

# Er-Doped $\text{LiNi}_{0.5}\text{Mn}_{1.5}\text{O}_4$ Cathode Material with Enhanced Cycling Stability for Lithium-Ion Batteries

Shanshan Liu <sup>1</sup>, Hongyuan Zhao <sup>1,\*</sup>, Ming Tan <sup>1</sup>, Youzuo Hu <sup>1</sup>, Xiaohui Shu <sup>1</sup>, Meiling Zhang <sup>1</sup>, Bing Chen <sup>1,2,\*</sup> and Xingquan Liu <sup>1,\*</sup>

<sup>1</sup> R&D Center for New Energy Materials and Devices, State Key Laboratory of Electronic Thin Film and Integrated Devices, University of Electronic Science and Technology of China, Chengdu 610054, China; shanshannay@163.com (S.L.); mingtan\_kilu@126.com (M.T.); huyouzuo@126.com (Y.H.); shu\_xh2016@163.com (X.S.); zhangmeiling199310@163.com (M.Z.)

<sup>2</sup> Xinyun Electronic Comp. & Dev. Co. Ltd, China Zhenhua Group, Guiyang 550018, China

\* Correspondence: hongyuanzhao@126.com (H.Z.); bchenuestc@126.com (B.C.); Lxquan@uestc.edu.cn (X.L.); Tel.: +86-28-832-06690 (X.L.)

Received: 28 June 2017; Accepted: 24 July 2017; Published: 27 July 2017

**Abstract:** The Er-doped  $\text{LiNi}_{0.5}\text{Mn}_{1.5}\text{O}_4$  ( $\text{LiNi}_{0.495}\text{Mn}_{1.495}\text{Er}_{0.01}\text{O}_4$ ) sample was successfully prepared by citric acid-assisted sol-gel method with erbium oxide as an erbium source for the first time. Compared with the undoped sample, the Er-doped  $\text{LiNi}_{0.5}\text{Mn}_{1.5}\text{O}_4$  sample maintained the basic spinel structure, suggesting that the substitution of  $\text{Er}^{3+}$  ions for partial nickel and manganese ions did not change the intrinsic structure of  $\text{LiNi}_{0.5}\text{Mn}_{1.5}\text{O}_4$ . Moreover, the Er-doped  $\text{LiNi}_{0.5}\text{Mn}_{1.5}\text{O}_4$  sample showed better size distribution and regular octahedral morphology. Electrochemical measurements indicated that the Er-doping could have a positive impact on the electrochemical properties. When cycled at 0.5 C, the Er-doped  $\text{LiNi}_{0.5}\text{Mn}_{1.5}\text{O}_4$  sample exhibited an initial discharge capacity of  $120.6 \text{ mAh}\cdot\text{g}^{-1}$ , and the capacity retention of this sample reached up to 92.9% after 100 cycles. As the charge/discharge rate restored from 2.0 C to 0.2 C, the discharge capacity of this sample still exhibited  $123.7 \text{ mAh}\cdot\text{g}^{-1}$  with excellent recovery rate. Since the bonding energy of Er-O ( $615 \text{ kJ}\cdot\text{mol}^{-1}$ ) was higher than that of Mn-O ( $402 \text{ kJ}\cdot\text{mol}^{-1}$ ) and Ni-O ( $392 \text{ kJ}\cdot\text{mol}^{-1}$ ), these outstanding performance could be attributed to the increased structure stability as well as the reduced aggregation behavior and small charge transfer resistance of the Er-doped  $\text{LiNi}_{0.5}\text{Mn}_{1.5}\text{O}_4$ .

**Keywords:** Lithium-ion battery;  $\text{LiNi}_{0.5}\text{Mn}_{1.5}\text{O}_4$ ; Er-doping; citric acid-assisted sol-gel method; cycling stability

## 1. Introduction

Lithium-ion batteries are widely believed to be the most promising power sources for next-generation electrical equipment. As an important component, cathode materials have a large impact on the electrochemical properties of lithium-ion batteries [1,2]. Up to now, researchers have developed several cathode materials, such as  $\text{LiCoO}_2$ ,  $\text{LiFePO}_4$ ,  $\text{LiMn}_2\text{O}_4$ , and  $\text{LiNi}_x\text{Co}_y\text{M}_z\text{O}_2$  ( $\text{M} = \text{Mn}, \text{Al}$ ), etc.

Among these commercial materials,  $\text{LiMn}_2\text{O}_4$  has broad development prospects because of the abundant manganese resource and environmental protection performance. However, this material presents poor cycling stability, especially at high temperature. For the derivatives of  $\text{LiMn}_2\text{O}_4$ , transition metal doped  $\text{LiM}_x\text{Mn}_{2-x}\text{O}_4$  ( $\text{M} = \text{Cu}$  [3],  $\text{Ni}$  [4],  $\text{Fe}$  [5],  $\text{Co}$  [6],  $\text{Cr}$  [7], etc.) cathode materials can exhibit a high voltage plateau at around 5.0 V, which creates a good condition for increasing the energy density and power density. Among them,  $\text{LiNi}_{0.5}\text{Mn}_{1.5}\text{O}_4$  has been recognized as the ideal high-voltage material due to the abundant nickel and manganese resources, eco-friendliness, low-cost, etc. [8–10]. As a result,  $\text{LiNi}_{0.5}\text{Mn}_{1.5}\text{O}_4$  has attracted much attention from academics and enterprises.

According to the existing literatures [11,12], the  $\text{LiNi}_{0.5}\text{Mn}_{1.5}\text{O}_4$  structure (disordered or ordered structure) depends on the ordering of nickel and manganese ions. Compared with the ordered sample, the disordered sample can show better electrochemical performance because of excellent electronic conductivity and low activation energy [13,14]. And the actual discharge capacity of this material can achieve about  $130 \text{ mAh}\cdot\text{g}^{-1}$ . Therefore,  $\text{LiNi}_{0.5}\text{Mn}_{1.5}\text{O}_4$  has great prospect in cathode materials for high-performance lithium-ion batteries. However, the commercial application of  $\text{LiNi}_{0.5}\text{Mn}_{1.5}\text{O}_4$  is restricted by some factors, such as the chemical dissolution of Mn, existence of  $\text{Li}_x\text{Ni}_{1-x}\text{O}$  impurities, oxidative decomposition of electrolyte working at high voltage and so on [15–17]. According to research results [18,19], doping technique can play an active role in modifying the  $\text{LiNi}_{0.5}\text{Mn}_{1.5}\text{O}_4$ . Liu et al. [20] have prepared the Er-doped  $\text{LiMn}_2\text{O}_4$  sample by the rheological phase reaction method. The Er-doped  $\text{LiMn}_2\text{O}_4$  can display good cycling stability, indicating that small amounts of  $\text{Er}^{3+}$  ions can promote the improvement of electrochemical properties. Moreover, the Er-doping also demonstrates a positive role in improving the cycling stability of other cathode materials such as  $\text{LiFePO}_4$  and  $\text{LiV}_3\text{O}_8$  [21,22]. Therefore, it is interesting to speculate that the substitution of  $\text{Er}^{3+}$  ions for partial nickel and manganese ions may show a positive effect on the electrochemical performance of  $\text{LiNi}_{0.5}\text{Mn}_{1.5}\text{O}_4$ .

In this work, the Er-doped  $\text{LiNi}_{0.5}\text{Mn}_{1.5}\text{O}_4$  was successfully prepared by the citric acid-assisted sol-gel method with erbium oxide as the erbium source for the first time. The substitution of  $\text{Er}^{3+}$  ions for partial nickel and manganese ions did not change the intrinsic structure of  $\text{LiNi}_{0.5}\text{Mn}_{1.5}\text{O}_4$ . Moreover, the Er-doped  $\text{LiNi}_{0.5}\text{Mn}_{1.5}\text{O}_4$  showed better size distribution and regular octahedral morphology. The effect of doping with  $\text{Er}^{3+}$  ions on the electrochemical performance of  $\text{LiNi}_{0.5}\text{Mn}_{1.5}\text{O}_4$  was studied in detail.

## 2. Experimental

The Er-doped  $\text{LiNi}_{0.5}\text{Mn}_{1.5}\text{O}_4$  ( $\text{LiNi}_{0.495}\text{Mn}_{1.495}\text{Er}_{0.01}\text{O}_4$ ) sample was successfully prepared by citric acid-assisted sol-gel method. Firstly, a certain amount of erbium oxide was suspended in concentrated nitric acid and continuously stirred for 30 mins. And then, the erbium oxide turbid liquid was refluxed at  $80^\circ\text{C}$  until a clear solution was obtained. The pink solution was shifted in a small beaker and evaporated to remove excess nitric acid. Subsequently, stoichiometric amounts of manganese acetate, nickel acetate, and erbium nitrate were dissolved in deionized water. The molar ratio of Li:Ni:Mn:Er:O was 1:0.495:1.495:0.01:4. The mixed solution of citric acid and lithium hydroxide was prepared and added to the former solution under stirring. Next, adding ammonia water manipulated the pH of the obtained solution to about 7.5. The achieved solution was evaporated at  $80^\circ\text{C}$  to get a wet greenish gel. After being dried at  $110^\circ\text{C}$  for 24 h in oven, the greenish gel was sintered at  $450^\circ\text{C}$  for 4 h in air. Subsequently, the decomposed gel precursor was ground in mortar and sintered at  $800^\circ\text{C}$  for 18 h in air to get the darkish product. The undoped  $\text{LiNi}_{0.5}\text{Mn}_{1.5}\text{O}_4$  sample was prepared by the same citric acid-assisted sol-gel technology.

In order to confirm the crystal structure, X-ray diffraction (XRD, Bruker DX-1000, Cu  $\text{K}\alpha$  radiation, Bruker Corporation, Karlsruhe, Germany) was carried out. The surface morphology of the  $\text{LiNi}_{0.5}\text{Mn}_{1.5}\text{O}_4$  and Er-doped  $\text{LiNi}_{0.5}\text{Mn}_{1.5}\text{O}_4$  samples was identified by scanning electron microscopy (SEM, Japanese Electronics Co., Ltd, Tokyo, Japan). For electrochemical evaluation, the working electrode was constituted from 85% synthesized product as cathode material, 10% acetylene black as conductive agent, and 5% polyvinylidene fluoride dissolved in N-methyl-2-pyrrolidone as binder. The working electrode was tested by using CR2025 coin-type cells. The electrode mixture was pasted on the aluminum foil and dried at  $100^\circ\text{C}$  for 30 min, and then compressed to obtain round positive plates. Lithium foil and polypropylene membrane were used as anode material and diaphragm, respectively. 1 M  $\text{LiPF}_6$  in a mixture ( $V_{\text{DMC}}:V_{\text{EMC}}:V_{\text{EC}} = 1:1:1$ ) was used as the electrolyte. Electrochemical measurements were carried out by using LAND CT2001A (Wuhan LAND Electronics Co., Ltd., Wuhan, China). Electrochemical impedance spectra (EIS) and cyclic voltammogram (CV) were studied by CS-350 electrochemical workstation (Wuhan Corrtest Instruments Corp., Ltd., Wuhan, China).

### 3. Results and Discussion

Figure 1 shows the XRD patterns of the  $\text{LiNi}_{0.5}\text{Mn}_{1.5}\text{O}_4$  and Er-doped  $\text{LiNi}_{0.5}\text{Mn}_{1.5}\text{O}_4$  samples. The characteristic diffraction peaks of the Er-doped  $\text{LiNi}_{0.5}\text{Mn}_{1.5}\text{O}_4$  sample are indexed to  $\text{LiNi}_{0.5}\text{Mn}_{1.5}\text{O}_4$  (JCPDS No. 80-2162) [23]. This indicates that the substitution of  $\text{Er}^{3+}$  ions for partial nickel and manganese ions has very little effect on the intrinsic structure [24–27]. Notably, the diffraction peaks show a small shift to smaller  $2\theta$  angle for the Er-doped  $\text{LiNi}_{0.5}\text{Mn}_{1.5}\text{O}_4$  sample with the introduction of a certain amount of  $\text{Er}^{3+}$  ions. This phenomenon can be interpreted as the successful incorporation of  $\text{Er}^{3+}$  ions into the crystal structure and an increase of the unit cell volume of the Er-doped  $\text{LiNi}_{0.5}\text{Mn}_{1.5}\text{O}_4$ . These results can be associated with the fact that the radius of  $\text{Er}^{3+}$  ions (1.04 Å) [20] is bigger than that of  $\text{Mn}^{4+}$  ions (0.53 Å) [25,26] and Ni ions (0.69 Å) [9]. According to the research results [18,27], if the dopant ions are located on the tetrahedral (8a) sites, the intensity of (220) peak, which arises only from the diffraction of the tetrahedral sites, must increase, even if the doping concentration is very low. From the Figure 1, it can be noted that the (220) peak does not appear in the XRD pattern of Er-doped  $\text{LiNi}_{0.5}\text{Mn}_{1.5}\text{O}_4$  sample. This indicates that the tetrahedral sites (8a) are occupied by  $\text{Li}^+$  ions, the  $\text{Er}^{3+}$  ions only occupy the octahedral (16d) sites to substitute nickel and manganese ions. Furthermore, the diffraction intensities of the Er-doped  $\text{LiNi}_{0.5}\text{Mn}_{1.5}\text{O}_4$  are stronger, which suggests that the substitution of  $\text{Er}^{3+}$  ions for partial nickel and manganese ions can enhance the crystallinity of  $\text{LiNi}_{0.5}\text{Mn}_{1.5}\text{O}_4$ .

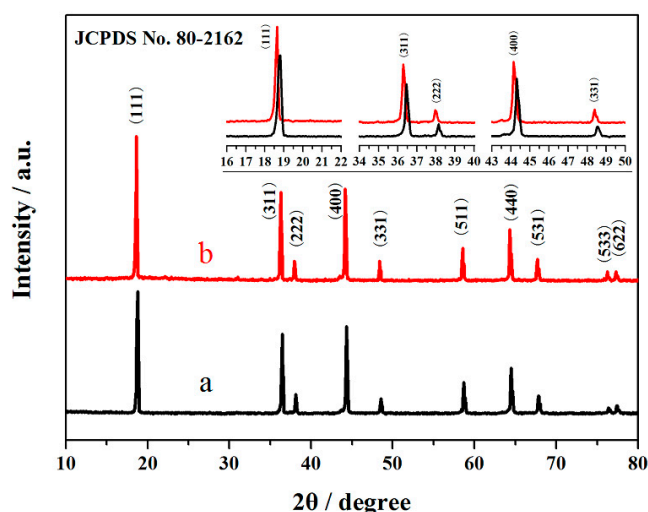


**Figure 1.** XRD patterns of the  $\text{LiNi}_{0.5}\text{Mn}_{1.5}\text{O}_4$  (a) and Er-doped  $\text{LiNi}_{0.5}\text{Mn}_{1.5}\text{O}_4$  (b).

Figure 2 shows the SEM images of the  $\text{LiNi}_{0.5}\text{Mn}_{1.5}\text{O}_4$  and Er-doped  $\text{LiNi}_{0.5}\text{Mn}_{1.5}\text{O}_4$  samples. As shown in Figure 2a, we can see that the undoped  $\text{LiNi}_{0.5}\text{Mn}_{1.5}\text{O}_4$  sample presents very undesirable grain size distribution with average particle size distribution of about 2.0  $\mu\text{m}$ . The smallest particle size is only 0.8  $\mu\text{m}$ , while the biggest particle size can reach up to about 5.0  $\mu\text{m}$ . By contrast, the Er-doped  $\text{LiNi}_{0.5}\text{Mn}_{1.5}\text{O}_4$  sample shown in Figure 2b exhibits better size distribution. Although the average particle size distribution is very close to that of the undoped  $\text{LiNi}_{0.5}\text{Mn}_{1.5}\text{O}_4$  sample, the biggest particle size has reduced to about 3.0  $\mu\text{m}$ . These results indicate that the substitution of  $\text{Er}^{3+}$  ions for partial nickel and manganese ions efficiently optimize the particle size distribution and reduces the aggregation behavior to some extent, which agrees with the research results [21,22]. According to the existing literature [21], the particle size of the Er-doped  $\text{LiFePO}_4$  powders is less than that of undoped  $\text{LiFePO}_4$  and the agglomeration of powders is decreased via Er doping in the lattice. Moreover, Xie et al. [22] has also confirmed the Er-doping can play an active role in optimizing the morphology of the Er-doped  $\text{LiV}_3\text{O}_8$  sample. Figure 3a,b show the energy dispersive spectrometry (EDS) pattern of the undoped  $\text{LiNi}_{0.5}\text{Mn}_{1.5}\text{O}_4$  and Er-doped  $\text{LiNi}_{0.5}\text{Mn}_{1.5}\text{O}_4$  sample (the inset in

Figure 3a,b is corresponding EDS data). According to Figure 3a,b, we can clearly observe the presence of the erbium element in the Er-doped  $\text{LiNi}_{0.5}\text{Mn}_{1.5}\text{O}_4$  sample. It should be noted that the signal strength of Er element is very small compared with Mn element, which can be attributed to the very low content of Er element. According to the ICP-OES result, the real compositions of the Er-doped  $\text{LiNi}_{0.5}\text{Mn}_{1.5}\text{O}_4$  sample is  $\text{Li}_{0.997}\text{Ni}_{0.494}\text{Mn}_{1.497}\text{Er}_{0.009}\text{O}_{4.000}$ . Such low content can help explain why the signal strength of Er element is very small. The corresponding EDS data of these two samples in Figure 3a,b also illuminates the low content of Er element. Moreover, the elemental mapping images of Ni, Mn, Er, and O elements of this material are shown in Figure 3c–f. It can be seen that the erbium element is evenly distributed in the Er-doped  $\text{LiNi}_{0.5}\text{Mn}_{1.5}\text{O}_4$  sample. The above results indicate that the Er-doping can play a significant role in the optimization of product size distribution. The obtained Er-doped  $\text{LiNi}_{0.5}\text{Mn}_{1.5}\text{O}_4$  sample may show excellent electrochemical properties.

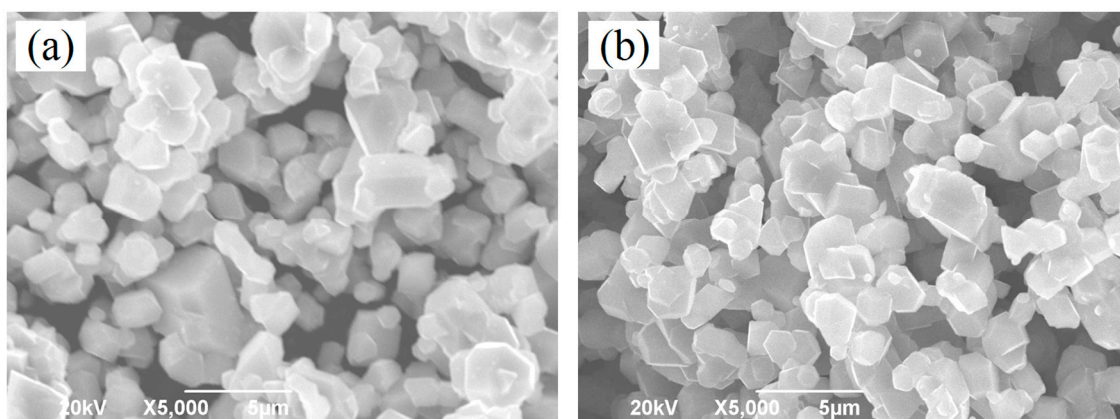


Figure 2. SEM images of the  $\text{LiNi}_{0.5}\text{Mn}_{1.5}\text{O}_4$  (a) and Er-doped  $\text{LiNi}_{0.5}\text{Mn}_{1.5}\text{O}_4$  (b).

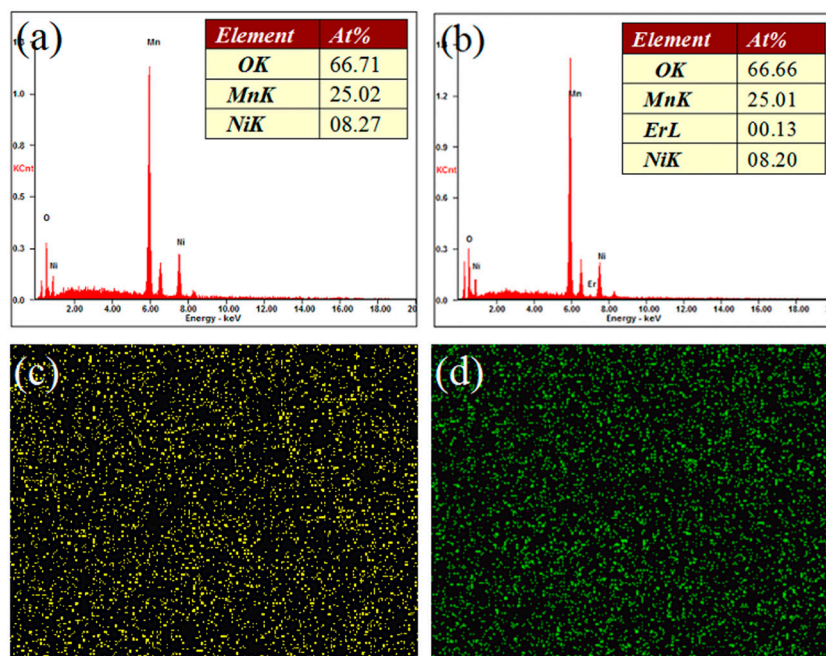
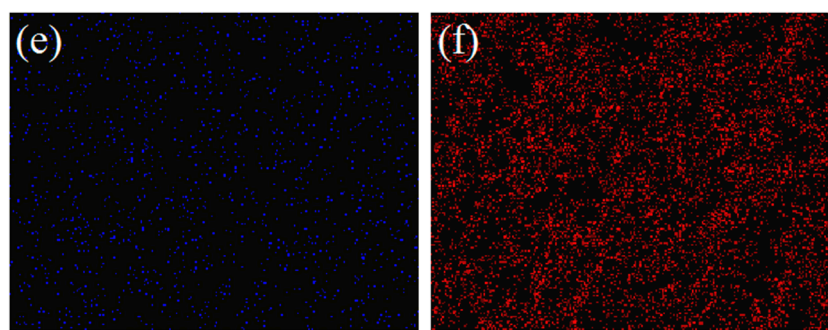


Figure 3. Cont.





**Figure 3.** Energy dispersive spectrometry (EDS) patterns of the undoped  $\text{LiNi}_{0.5}\text{Mn}_{1.5}\text{O}_4$  (a) and Er-doped  $\text{LiNi}_{0.5}\text{Mn}_{1.5}\text{O}_4$  (b) sample (The inset in Figure 3a,b is corresponding EDS data); (c–f) Elemental mapping images of Ni, Mn, Er, and O elements in the Er-doped  $\text{LiNi}_{0.5}\text{Mn}_{1.5}\text{O}_4$  sample.

To compare the effect of doping with  $\text{Er}^{3+}$  ions on the cycling stability, the  $\text{LiNi}_{0.5}\text{Mn}_{1.5}\text{O}_4$  and Er-doped  $\text{LiNi}_{0.5}\text{Mn}_{1.5}\text{O}_4$  samples were cycled at 0.5 C between 3.6 and 4.9 V. Figure 4a,b shows the representative charge/discharge curves of these two materials. As shown here, the charge/discharge curves of these two samples have a high similarity in the shape of these curves, suggesting that the substitution of  $\text{Er}^{3+}$  ions for partial nickel and manganese ions does not produce a fundamental impact on the insertion/deinsertion process of lithium ions. The Er-doped  $\text{LiNi}_{0.5}\text{Mn}_{1.5}\text{O}_4$  sample presents two obvious plateaus at around 4.7 V and 4.0 V, which agrees well with that of disordered  $\text{LiNi}_{0.5}\text{Mn}_{1.5}\text{O}_4$  in the literatures [26,27]. These two plateaus can be ascribed to the redox reaction of  $\text{Ni}^{2+/4+}$  and  $\text{Mn}^{3+/4+}$ , respectively. Figure 4c,d shows the cycling performances of these two materials. According to Figure 4d, the initial discharge capacity of the Er-doped  $\text{LiNi}_{0.5}\text{Mn}_{1.5}\text{O}_4$  sample is  $120.6 \text{ mAh}\cdot\text{g}^{-1}$ , which is slightly lower than that of the undoped  $\text{LiNi}_{0.5}\text{Mn}_{1.5}\text{O}_4$  sample ( $124.5 \text{ mAh}\cdot\text{g}^{-1}$ ). However, it is important to note that the initial discharge capacity of the undoped  $\text{LiNi}_{0.5}\text{Mn}_{1.5}\text{O}_4$  sample begins to fade greatly with the cycling going on. After 30 cycles, the Er-doped  $\text{LiNi}_{0.5}\text{Mn}_{1.5}\text{O}_4$  sample present excellent capacity retention of 93.2%. By contrast, the undoped sample shows very low capacity retention (64.5%). These results indicate that the Er-doping effectively promote the improvement of cycling stability.

In order to investigate the cycling stability, the long cycling performance of the Er-doped  $\text{LiNi}_{0.5}\text{Mn}_{1.5}\text{O}_4$  sample was carried out at 0.5 C, as shown in Figure 5a. The Er-doped  $\text{LiNi}_{0.5}\text{Mn}_{1.5}\text{O}_4$  sample still achieves more than  $112.0 \text{ mAh}\cdot\text{g}^{-1}$  and the capacity retention of this sample reach up to 92.9% after 100 cycles. By contrast, the cycling stability of the undoped  $\text{LiNi}_{0.5}\text{Mn}_{1.5}\text{O}_4$  sample is much worse. It delivers the bad capacity retention of 70.9% after only 30 cycles. The excellent cycling stability of the Er-doped  $\text{LiNi}_{0.5}\text{Mn}_{1.5}\text{O}_4$  sample is linked most strongly with the substitution of  $\text{Er}^{3+}$  ions for partial nickel and manganese ions in the spinel structure. For the Er-doped sample, the bonding energy of Er-O ( $615 \text{ kJ}\cdot\text{mol}^{-1}$ ) is higher than that of Mn-O ( $402 \text{ kJ}\cdot\text{mol}^{-1}$ ) and Ni-O ( $392 \text{ kJ}\cdot\text{mol}^{-1}$ ), which can make the spinel structure of the Er-doped  $\text{LiNi}_{0.5}\text{Mn}_{1.5}\text{O}_4$  sample become more stable [9,20,26]. Figure 5b shows the coulombic efficiency of the Er-doped  $\text{LiNi}_{0.5}\text{Mn}_{1.5}\text{O}_4$  sample after 100 cycles. As shown here, the coulombic efficiency of the initial cycle is about 93.6%, which can be explained by the side reactions of electrolyte and electrode working at high voltage [28]. As the increase of the charge/discharge cycle, the coulombic efficiency is increased to 95.4% after 3 cycles and 98.6% after 30 cycles. Such improved cycling efficiency can be ascribed to the stable solid electrolyte interphase (SEI) on the spinel after the initial cycle, which can hinder the further side reactions [29].

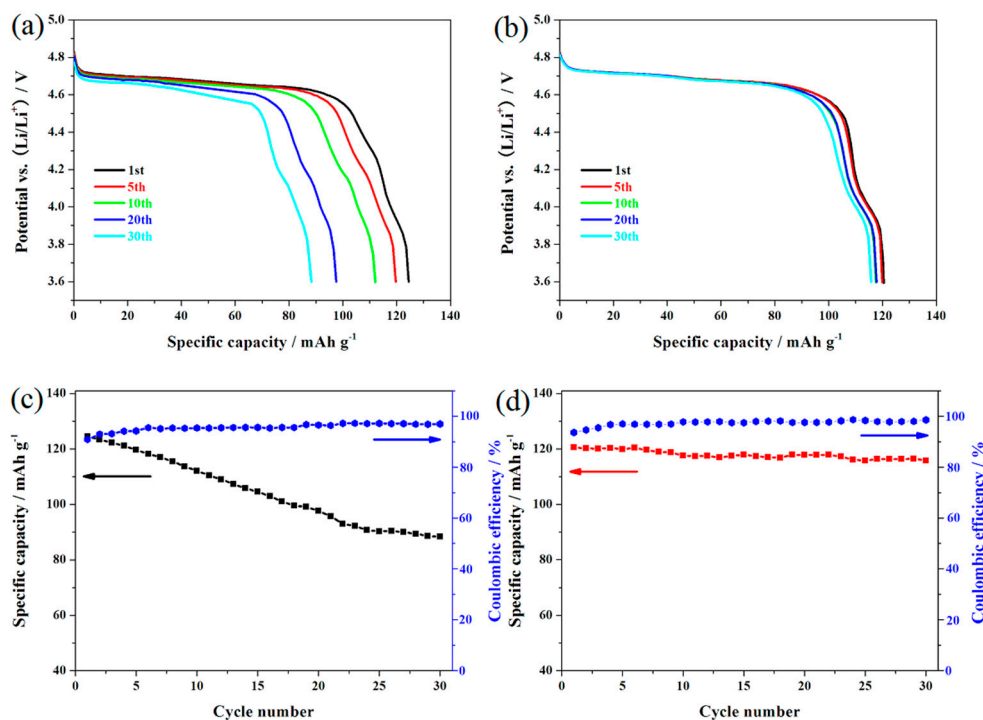


**Figure 4.** Representative charge/discharge curves of the  $\text{LiNi}_{0.5}\text{Mn}_{1.5}\text{O}_4$  (a) and Er-doped  $\text{LiNi}_{0.5}\text{Mn}_{1.5}\text{O}_4$  (b); cycling performance and coulombic efficiency of the  $\text{LiNi}_{0.5}\text{Mn}_{1.5}\text{O}_4$  (c) and Er-doped  $\text{LiNi}_{0.5}\text{Mn}_{1.5}\text{O}_4$  (d).

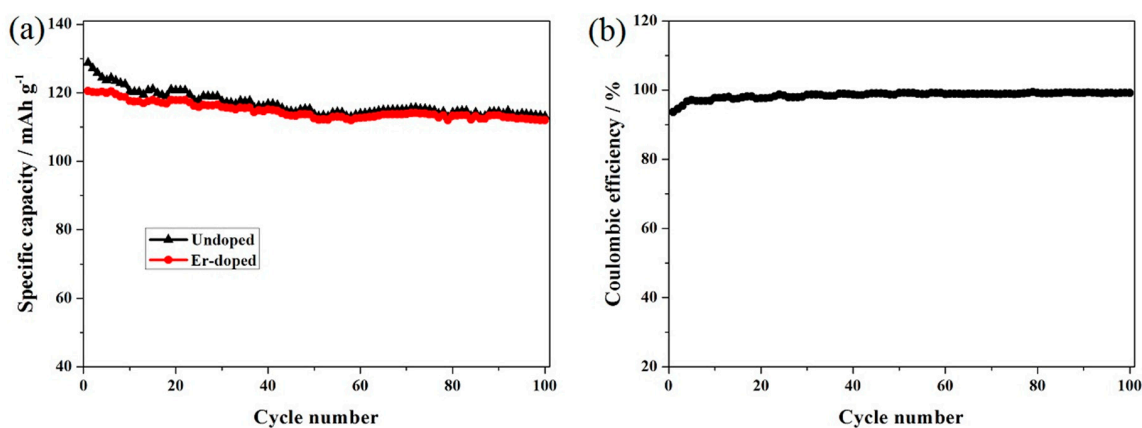


**Figure 5.** (a) Long cycling performance and (b) coulombic efficiency of the Er-doped  $\text{LiNi}_{0.5}\text{Mn}_{1.5}\text{O}_4$  at 0.5 C.

Figure 6a,b shows the representative discharge curves of the  $\text{LiNi}_{0.5}\text{Mn}_{1.5}\text{O}_4$  and Er-doped  $\text{LiNi}_{0.5}\text{Mn}_{1.5}\text{O}_4$  samples at different rates. According to Figure 6a, the undoped  $\text{LiNi}_{0.5}\text{Mn}_{1.5}\text{O}_4$  sample presents a discharge capacity loss from  $130.2 \text{ mAh}\cdot\text{g}^{-1}$  at 0.2 C to  $64.7 \text{ mAh}\cdot\text{g}^{-1}$  at 2.0 C along with the obvious decrement of the discharge voltage plateaus. By contrast, the Er-doping significantly enhances the rate performance of the Er-doped  $\text{LiNi}_{0.5}\text{Mn}_{1.5}\text{O}_4$ . As shown in Figure 6b, the increased charge/discharge rate does not noticeably alter the representative discharge curve of the Er-doped  $\text{LiNi}_{0.5}\text{Mn}_{1.5}\text{O}_4$  sample. However, the discharge voltage plateaus of the spinel gradually decrease as the charge/discharge rate increases, which may be explained by the following two reasons. On the one hand, the higher rate can spur the increase in the polarization of cathode material, which will decrease the discharge voltage plateaus [18]. On the other hand, the increased essential resistance can cause an obvious voltage drop when lithium-ion battery is cycled at higher rate [30].

Figure 6c shows the cycling stability of the  $\text{LiNi}_{0.5}\text{Mn}_{1.5}\text{O}_4$  and Er-doped  $\text{LiNi}_{0.5}\text{Mn}_{1.5}\text{O}_4$  samples at different rates from 0.2 C to 2.0 C. As might be expected, the increase of discharge rate decreases the discharge capacity for both samples due to the limited lithium ions diffusion [31]. The Er-doped  $\text{LiNi}_{0.5}\text{Mn}_{1.5}\text{O}_4$  sample shows more prominent rate capability, especially the higher rate performance. When cycled at 0.2 C, the Er-doped  $\text{LiNi}_{0.5}\text{Mn}_{1.5}\text{O}_4$  sample presents  $125.4 \text{ mAh}\cdot\text{g}^{-1}$ . As the charge/discharge rate increases to 2.0 C, the discharge capacity of this material can still retain  $102.1 \text{ mAh}\cdot\text{g}^{-1}$ , which is 81.4% of its initial discharge capacity cycled at 0.2 C. However, the undoped  $\text{LiNi}_{0.5}\text{Mn}_{1.5}\text{O}_4$  spinel only retains 49.7% at 2.0 C. In addition, when the rate restores to 0.2 C, the Er-doped  $\text{LiNi}_{0.5}\text{Mn}_{1.5}\text{O}_4$  sample delivers  $123.7 \text{ mAh}\cdot\text{g}^{-1}$  with excellent recovery rate. Figure 6d shows the cycling stability of the Er-doped  $\text{LiNi}_{0.5}\text{Mn}_{1.5}\text{O}_4$  sample at 2.0 C. it can be seen that the Er-doped  $\text{LiNi}_{0.5}\text{Mn}_{1.5}\text{O}_4$  sample exhibits an initial discharge capacity of  $100.4 \text{ mAh}\cdot\text{g}^{-1}$ , and the capacity retention of this sample reached up to 97.6% after 30 cycles. The analysis results once again prove that the electrochemical performance of spinel  $\text{LiNi}_{0.5}\text{Mn}_{1.5}\text{O}_4$  can be greatly enhanced by the addition of  $\text{Er}^{3+}$  ions.

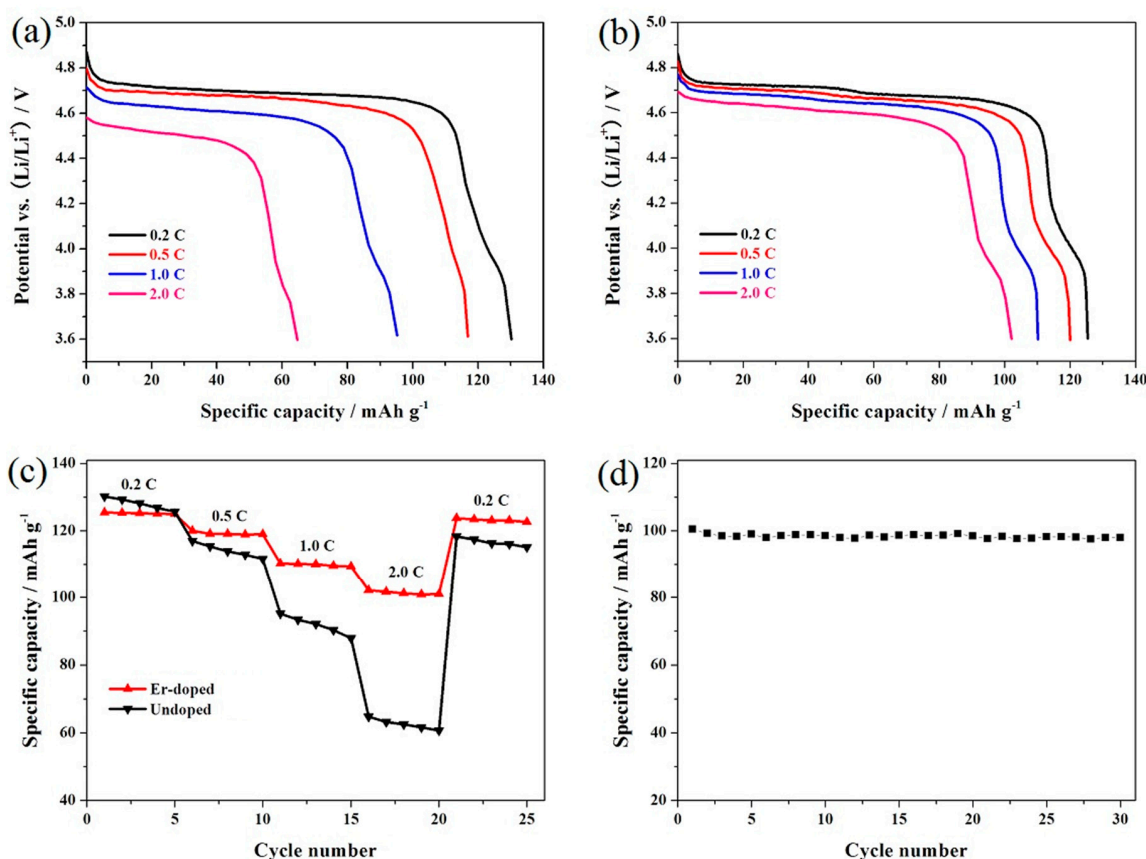


**Figure 6.** Representative discharge curves of the  $\text{LiNi}_{0.5}\text{Mn}_{1.5}\text{O}_4$  (a) and Er-doped  $\text{LiNi}_{0.5}\text{Mn}_{1.5}\text{O}_4$  (b) at different rates; (c) rate capability of the  $\text{LiNi}_{0.5}\text{Mn}_{1.5}\text{O}_4$  and Er-doped  $\text{LiNi}_{0.5}\text{Mn}_{1.5}\text{O}_4$ ; (d) cycling stability of the Er-doped  $\text{LiNi}_{0.5}\text{Mn}_{1.5}\text{O}_4$  at 2.0 C.

Figure 7 shows the cycling performance of the  $\text{LiNi}_{0.5}\text{Mn}_{1.5}\text{O}_4$  and Er-doped  $\text{LiNi}_{0.5}\text{Mn}_{1.5}\text{O}_4$  samples at  $55^\circ\text{C}$ . When cycled at 0.5 C, the Er-doped  $\text{LiNi}_{0.5}\text{Mn}_{1.5}\text{O}_4$  sample exhibits an initial discharge capacity of  $120.3 \text{ mAh}\cdot\text{g}^{-1}$ , which is slightly lower than that of the undoped  $\text{LiNi}_{0.5}\text{Mn}_{1.5}\text{O}_4$  sample ( $124.3 \text{ mAh}\cdot\text{g}^{-1}$ ). However, after 30 cycles, the Er-doped  $\text{LiNi}_{0.5}\text{Mn}_{1.5}\text{O}_4$  sample still delivers  $113.7 \text{ mAh}\cdot\text{g}^{-1}$ , retaining 94.5% of its initial discharge capacity. Contemporaneously, the undoped  $\text{LiNi}_{0.5}\text{Mn}_{1.5}\text{O}_4$  sample retains just 58.1%. Figure 8a,b shows the representative discharge curves of the  $\text{LiNi}_{0.5}\text{Mn}_{1.5}\text{O}_4$  and Er-doped  $\text{LiNi}_{0.5}\text{Mn}_{1.5}\text{O}_4$  at  $55^\circ\text{C}$ . The initial discharge curves of these two

samples have a high similarity in the shape of these curves, but the corresponding 30th discharge curves present obvious difference. For the Er-doped  $\text{LiNi}_{0.5}\text{Mn}_{1.5}\text{O}_4$  sample, there is no discharge voltage drop after 30 cycles, while the discharge voltage drop of the undoped  $\text{LiNi}_{0.5}\text{Mn}_{1.5}\text{O}_4$  sample is quite obvious. The above result shows that the addition of  $\text{Er}^{3+}$  can enhance the cycling stability of  $\text{LiNi}_{0.5}\text{Mn}_{1.5}\text{O}_4$  at elevated-temperature.

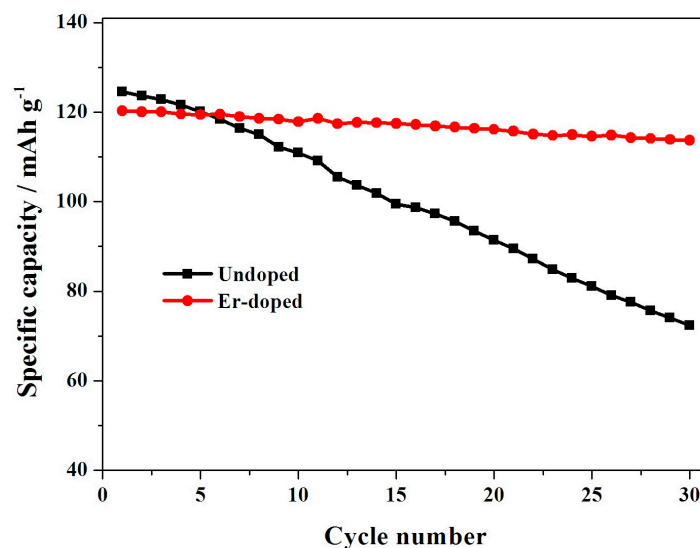


Figure 7. Cycling performance of the  $\text{LiNi}_{0.5}\text{Mn}_{1.5}\text{O}_4$  and Er-doped  $\text{LiNi}_{0.5}\text{Mn}_{1.5}\text{O}_4$  at 55 °C.

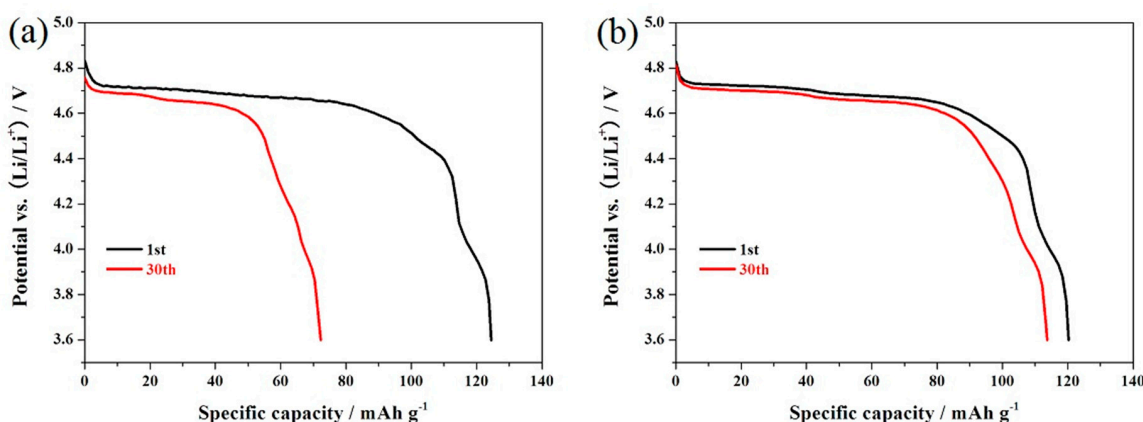
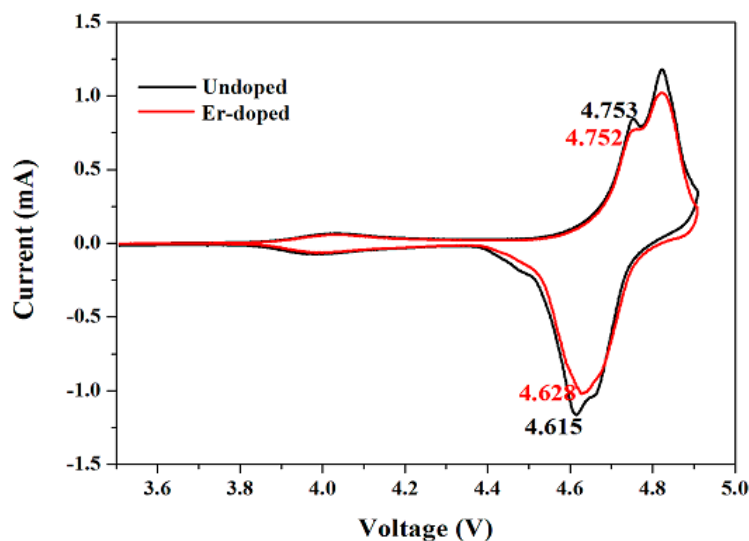


Figure 8. Representative discharge curves of the  $\text{LiNi}_{0.5}\text{Mn}_{1.5}\text{O}_4$  (a) and Er-doped  $\text{LiNi}_{0.5}\text{Mn}_{1.5}\text{O}_4$  (b) at 55 °C.

Figure 9 shows the cyclic voltammograms of the  $\text{LiNi}_{0.5}\text{Mn}_{1.5}\text{O}_4$  and Er-doped  $\text{LiNi}_{0.5}\text{Mn}_{1.5}\text{O}_4$  samples. The scan rate is  $0.1 \text{ mV} \cdot \text{s}^{-1}$  and the scanning voltage is from 3.5 to 4.9 V. It can be clearly observed that these two samples present three pairs of reduction and oxidation peaks. Among them, the small reduction and oxidation peaks at around 4.0 V suggests the redox reaction of  $\text{Mn}^{3+/4+}$  couples [32]. And the main two pairs of redox peaks at around 4.7 V are ascribed to redox reactions of  $\text{Ni}^{2+/3+}$  and  $\text{Ni}^{3+/4+}$ , respectively [33]. From the redox peaks of  $\text{Ni}^{2+/3+}$  of the two samples, we can find that the Er-doped  $\text{LiNi}_{0.5}\text{Mn}_{1.5}\text{O}_4$  sample presents a little smaller anodic peak and a much higher cathodic peak than the undoped  $\text{LiNi}_{0.5}\text{Mn}_{1.5}\text{O}_4$  sample. Such much smaller difference suggests a higher reversibility of electrode reaction [34].





**Figure 9.** Cyclic voltammograms of the  $\text{LiNi}_{0.5}\text{Mn}_{1.5}\text{O}_4$  and Er-doped  $\text{LiNi}_{0.5}\text{Mn}_{1.5}\text{O}_4$  in the range of 3.5–4.9 V.

Figure 10 shows the Nyquist plots of the  $\text{LiNi}_{0.5}\text{Mn}_{1.5}\text{O}_4$  and Er-doped  $\text{LiNi}_{0.5}\text{Mn}_{1.5}\text{O}_4$  samples. The possible equivalent circuit model is embedded in Figure 10, where  $R_e$  and  $R_{ct}$  represent the ohmic resistance and charge transfer resistance, respectively [35,36]. And the fitting results of impedance parameters are listed in Table 1. Between the two kinds of resistances, the charge transfer resistance is much related to electrochemical property of electrode material [37]. The undoped  $\text{LiNi}_{0.5}\text{Mn}_{1.5}\text{O}_4$  sample displays a high charge transfer resistance of 377.1  $\Omega$ . However, after the addition of  $\text{Er}^{3+}$ , the charge transfer resistance is decreased to 210.8  $\Omega$ , which makes it much easier for lithium-ion diffusion during the process of charge/discharge. Therefore, it should make sense why the Er-doped  $\text{LiNi}_{0.5}\text{Mn}_{1.5}\text{O}_4$  spinel presents better electrochemical property.

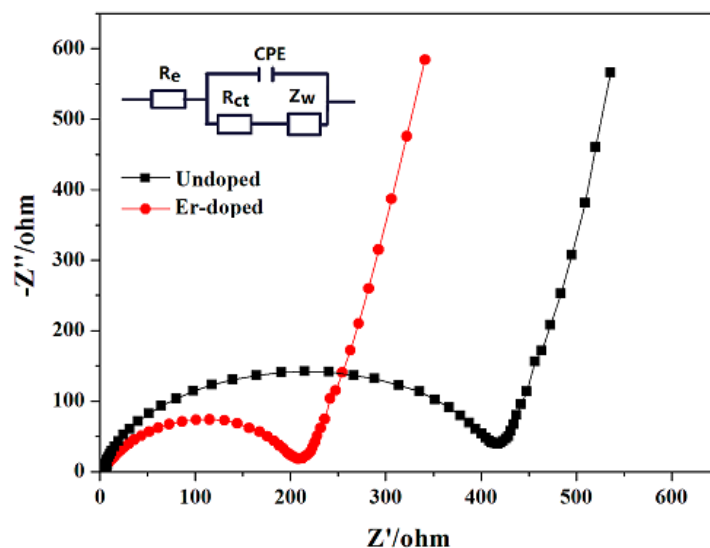


**Figure 10.** Nyquist plots of the  $\text{LiNi}_{0.5}\text{Mn}_{1.5}\text{O}_4$  and Er-doped  $\text{LiNi}_{0.5}\text{Mn}_{1.5}\text{O}_4$  before cycles (the insert is the equivalent circuit model of EIS).

**Table 1.** Impedance fitted data from EIS spectra for the  $\text{LiNi}_{0.5}\text{Mn}_{1.5}\text{O}_4$  and Er-doped  $\text{LiNi}_{0.5}\text{Mn}_{1.5}\text{O}_4$ .

Sample	$R_e$ ( $\Omega$ )	$R_{ct}$ ( $\Omega$ )
$\text{LiNi}_{0.5}\text{Mn}_{1.5}\text{O}_4$	4.01	377.13
Er-doped $\text{LiNi}_{0.5}\text{Mn}_{1.5}\text{O}_4$	3.04	210.81

#### 4. Conclusions

The Er-doped  $\text{LiNi}_{0.5}\text{Mn}_{1.5}\text{O}_4$  sample was successfully prepared by the citric acid-assisted sol-gel method with erbium oxide as erbium source for the first time. XRD and SEM characterization indicated that the substitution of  $\text{Er}^{3+}$  ions for partial nickel and manganese ions did not change the intrinsic structure of  $\text{LiNi}_{0.5}\text{Mn}_{1.5}\text{O}_4$  and the Er-doped  $\text{LiNi}_{0.5}\text{Mn}_{1.5}\text{O}_4$  sample showed better size distribution and regular octahedral morphology. When cycled at 0.5 C, the Er-doped  $\text{LiNi}_{0.5}\text{Mn}_{1.5}\text{O}_4$  sample exhibited an initial discharge capacity of  $120.6 \text{ mAh}\cdot\text{g}^{-1}$ , and the capacity retention of this sample reached up to 92.9% after 100 cycles. Furthermore, it could show excellent recovery rate, superior rate capability, and good high-temperature performance. The above results indicate that the substitution of  $\text{Er}^{3+}$  ions for partial nickel and manganese ions can play an active role in modifying  $\text{LiNi}_{0.5}\text{Mn}_{1.5}\text{O}_4$ .

**Acknowledgments:** The authors appreciate the financial support from the National Natural Science Foundation of China (grant No. 21071026).

**Author Contributions:** Hongyuan Zhao, Bing Chen, and Xingquan Liu conceived and designed the experiments; Shanshan Liu and Hongyuan Zhao performed the experiments; all authors analyzed the data; Shanshan Liu and Hongyuan Zhao co-wrote the paper; all authors discussed the results and commented on the paper.

**Conflicts of Interest:** The authors declare no conflicts of interest.

#### References

1. Fergus, J.W. Recent developments in cathode materials for lithium ion batteries. *J. Power Sources* **2010**, *195*, 939–954. [[CrossRef](#)]
2. Cheng, J.; Li, X.; Wang, Z.; Guo, H. Hydrothermal synthesis of  $\text{LiNi}_{0.5}\text{Mn}_{1.5}\text{O}_4$  sphere and its performance as high-voltage cathode material for lithium ion batteries. *Ceram. Int.* **2016**, *42*, 3715–3719. [[CrossRef](#)]
3. Sulochana, A.; Thirunakaran, R.; Sivashanmugam, A.; Gopukumar, S.; Yamkiet, J. Sol-gel synthesis of 5 V  $\text{LiCu}_x\text{Mn}_{2-x}\text{O}_4$  as a cathode material for lithium rechargeable batteries. *J. Electrochem. Soc.* **2008**, *155*, A206–A210. [[CrossRef](#)]
4. Wei, Y.J.; Yan, L.Y.; Wang, C.Z.; Xu, X.G.; Wu, F.; Chen, G. Effect of Ni doping on  $[\text{MnO}_6]$  octahedron in  $\text{LiMn}_2\text{O}_4$ . *J. Phys. Chem. B* **2004**, *108*, 18547–18551. [[CrossRef](#)]
5. Shigemura, H.; Sakaebe, H.; Kageyama, H.; Kobayashi, H.; West, A.R.; Kanno, R.; Morimoto, S.; Nasu, S.; Tabuchi, M. Structure and electrochemical properties of  $\text{LiFe}_x\text{Mn}_{2-x}\text{O}_4$  ( $0 \leq x \leq 0.5$ ) spinel as 5 V electrode material for lithium batteries. *J. Electrochem. Soc.* **2001**, *148*, A730–A736. [[CrossRef](#)]
6. Mandal, S.; Rojas, R.M.; Amarilla, J.M.; Calle, P.; Kosova, N.V.; Anufrienko, V.F.; Rojo, J.M. High temperature co-doped  $\text{LiMn}_2\text{O}_4$ -based spinels. structural, electrical, and electrochemical characterization. *Chem. Mater.* **2002**, *14*, 1598–1605. [[CrossRef](#)]
7. Sigala, C.; Guyomard, D.; Verbaere, A.; Piffard, Y.; Tournoux, M. Positive electrode materials with high operating voltage for lithium batteries:  $\text{LiCr}_y\text{Mn}_{2-y}\text{O}_4$  ( $0 \leq y \leq 1$ ). *Solid State Ionics* **1995**, *81*, 167–170. [[CrossRef](#)]
8. Kanamura, K.; Hoshikawa, W.; Umegaki, T. Electrochemical characteristics of  $\text{LiNi}_{0.5}\text{Mn}_{1.5}\text{O}_4$  cathodes with Ti or Al current collectors. *J. Electrochem. Soc.* **2002**, *149*, A339–A345. [[CrossRef](#)]
9. Yi, T.F.; Zhu, Y.R.; Zhu, R.S. Density functional theory study of lithium intercalation for 5 V  $\text{LiNi}_{0.5}\text{Mn}_{1.5}\text{O}_4$  cathode materials. *Solid State Ionics* **2008**, *179*, 2132–2136. [[CrossRef](#)]
10. Bae, S.Y.; Shin, W.K.; Kim, D.W. Protective organic additives for high voltage  $\text{LiNi}_{0.5}\text{Mn}_{1.5}\text{O}_4$  cathode materials. *Electrochim. Acta* **2014**, *125*, 497–502. [[CrossRef](#)]
11. Idemoto, Y.; Narai, H.; Koura, N. Crystal structure and cathode performance dependence on oxygen content of  $\text{LiMn}_{1.5}\text{Ni}_{0.5}\text{O}_4$  as a cathode material for secondary lithium batteries. *J. Power Sources* **2003**, *119*, 125–129. [[CrossRef](#)]

12. Kunduraci, M.; Amatucci, G.G. Synthesis and characterization of nanostructured 4.7 V  $\text{Li}_x\text{Mn}_{1.5}\text{Ni}_{0.5}\text{O}_4$  spinels for high-power lithium-ion batteries. *J. Electrochem. Soc.* **2006**, *153*, A1345–A1352. [[CrossRef](#)]
13. Kunduraci, M.; Al-Sharab, J.F.; Amatucci, G.G. High-power nanostructured  $\text{LiMn}_{2-x}\text{Ni}_x\text{O}_4$  high-voltage lithium-ion battery electrode materials: Electrochemical impact of electronic conductivity and morphology. *Chem. Mater.* **2006**, *18*, 3585–3592. [[CrossRef](#)]
14. Ma, X.H.; Kang, B.; Ceder, G. High rate micron-sized ordered  $\text{LiNi}_{0.5}\text{Mn}_{1.5}\text{O}_4$ . *J. Electrochem. Soc.* **2010**, *157*, A925–A931. [[CrossRef](#)]
15. Yoon, T.; Park, S.; Mun, J.; Ji, H.R.; Choi, W. Failure mechanisms of  $\text{LiNi}_{0.5}\text{Mn}_{1.5}\text{O}_4$  electrode at elevated temperature. *J. Power Sources* **2012**, *215*, 312–316. [[CrossRef](#)]
16. Jin, Y.C.; Lin, C.Y.; Duh, J.G. Improving rate capability of high potential  $\text{LiNi}_{0.5}\text{Mn}_{1.5}\text{O}_{4-x}$  cathode materials via increasing oxygen non-stoichiometries. *Electrochim. Acta* **2012**, *69*, 45–50. [[CrossRef](#)]
17. Xu, W.; Chen, X.; Ding, F.; Xiao, J.; Wang, D.Y.; Pan, A.Q.; Zheng, J.M.; Li, X.H.S.; Padmaperuma, A.B.; Zhang, J.G. Reinvestigation on the state-of-the-art nonaqueous carbonate electrolytes for 5 V Li-ion battery applications. *J. Power Sources* **2012**, *213*, 304–316. [[CrossRef](#)]
18. Zhao, H.Y.; Liu, X.Q.; Cheng, C.; Li, Q.; Zhang, Z.; Wu, Y.; Chen, B.; Xiong, W. Synthesis and electrochemical characterizations of spinel  $\text{LiMn}_{1.94}\text{MO}_4$  ( $\text{M} = \text{Mn}_{0.06}, \text{Mg}_{0.06}, \text{Si}_{0.06}, (\text{Mg}_{0.03}\text{Si}_{0.03})$ ) compounds as cathode materials for lithium-ion batteries. *J. Power Sources* **2015**, *282*, 118–128. [[CrossRef](#)]
19. Aklalouch, M.; Amarilla, J.M.; Rojas, R.M.; Saadoune, I.; Rojo, J.M. Chromium doping as a new approach to improve the cycling performance at high temperature of 5 V  $\text{LiNi}_{0.5}\text{Mn}_{1.5}\text{O}_4$ -based positive electrode. *J. Power Sources* **2008**, *185*, 501–511. [[CrossRef](#)]
20. Liu, H.W.; Zhang, K.L. The synthesis and cycling behavior of  $\text{LiEr}_x\text{Mn}_{2-x}\text{O}_4$  for lithium-ion batteries. *Mater. Lett.* **2004**, *58*, 3049–3051. [[CrossRef](#)]
21. Göktepe, H.; Sahan, H.; Ülgen, A.; Patat, S. Synthesis and electrochemical properties of carbon-mixed  $\text{LiEr}_{0.02}\text{Fe}_{0.98}\text{PO}_4$  cathode material for lithium-ion batteries. *J. Mater. Sci. Technol.* **2011**, *27*, 861–864. [[CrossRef](#)]
22. Xie, L.L.; Xu, Y.D.; Zhang, J.J.; Zhang, C.; Cao, X.; Qu, L. Rheological phase synthesis of Er-doped  $\text{LiV}_3\text{O}_8$  as electroactive material for a cathode of secondary lithium storage. *Electron. Mater. Lett.* **2013**, *9*, 549–553. [[CrossRef](#)]
23. Dong, Y.; Young, B.T.; Zhang, Y.; Yoon, T.; Heskett, D.R.; Hu, Y.; Lucht, B.L. Effect of lithium borate additives on cathode film formation in  $\text{LiNi}_{0.5}\text{Mn}_{1.5}\text{O}_4/\text{Li}$  cells. *ACS Appl. Mater. Interfaces* **2017**, *9*, 20467–20475. [[CrossRef](#)] [[PubMed](#)]
24. Chung, H.T.; Myung, S.T.; Cho, T.H.; Son, J.T. Lattice parameter as a measure of electrochemical properties of  $\text{LiMn}_2\text{O}_4$ . *J. Power Sources* **2001**, *97*, 454–457. [[CrossRef](#)]
25. Feng, F.; Liang, C.; Fang, H.; Yang, B.; Ma, W.; Dai, Y. Chloride-promoted formation of octahedral  $\text{LiNi}_{0.5}\text{Mn}_{1.5}\text{O}_4$  crystal with greatly enhanced electrochemical performance. *Ceram. Int.* **2016**, *42*, 9038–9045. [[CrossRef](#)]
26. Mo, M.; Hui, K.; Hong, X.; Guo, J.; Ye, C.; Li, A.; Hu, N.; Huang, Z.; Jiang, J.; Liang, J.; et al. Improved cycling and rate performance of Sm-doped  $\text{LiNi}_{0.5}\text{Mn}_{1.5}\text{O}_4$  cathode materials for 5 V lithium ion batteries. *Appl. Surf. Sci.* **2014**, *290*, 412–418. [[CrossRef](#)]
27. Arunkumar, T.A.; Manthiram, A. Influence of chromium doping on the electrochemical performance of the 5 V spinel cathode  $\text{LiMn}_{1.5}\text{Ni}_{0.5}\text{O}_4$ . *Electrochim. Acta* **2005**, *50*, 5568–5572. [[CrossRef](#)]
28. Wu, H.M.; Tu, J.P.; Yuan, Y.F.; Li, Y.; Zhao, X.B.; Cao, G.S. Electrochemical and ex situ XRD studies of a  $\text{LiMn}_{1.5}\text{Ni}_{0.5}\text{O}_4$  high-voltage cathode material. *Electrochim. Acta* **2005**, *50*, 4104–4108. [[CrossRef](#)]
29. Wen, J.W.; Zhang, D.W.; Zhang, Y.; Sun, X.; Cheng, B.; Ding, C.X.; Yu, Y.; Chen, C.H. One-step synthesis and effect of heat-treatment on the structure and electrochemical properties of  $\text{LiNi}_{0.5}\text{Mn}_{1.5}\text{O}_4$  cathode material for lithium-ion batteries. *Electrochim. Acta* **2014**, *133*, 515–521. [[CrossRef](#)]
30. Li, B.; Wang, Y.; Tu, W.; Wang, Z.; Xi, M.; Xing, L.; Li, W. Improving cyclic stability of lithium nickel manganese oxide cathode for high voltage lithium ion battery by modifying electrode/electrolyte interface with electrolyte additive. *Electrochim. Acta* **2014**, *147*, 636–642. [[CrossRef](#)]
31. Yi, T.F.; Xie, Y.; Zhu, Y.R.; Zhu, R.S.; Ye, M.F. High rate micron-sized niobium-doped  $\text{LiMn}_{1.5}\text{Ni}_{0.5}\text{O}_4$  as ultra high power positive-electrode material for lithium-ion batteries. *J. Power Sources* **2012**, *211*, 59–65. [[CrossRef](#)]

32. Ding, Y.L.; Xie, J.; Cao, G.S.; Zhu, T.J.; Yu, H.M.; Zhao, X.B. Single-crystalline  $\text{LiMn}_2\text{O}_4$  nanotubes synthesized via template-engaged reaction as cathodes for high-power lithium ion batteries. *Adv. Funct. Mater.* **2011**, *21*, 348–355. [[CrossRef](#)]
33. Xiong, L.L.; Xu, Y.L.; Tao, T.; Goodenough, J.B. Synthesis and electrochemical characterization of multi-cations doped spinel  $\text{LiMn}_2\text{O}_4$  used for lithium ion batteries. *J. Power Sources* **2012**, *199*, 214–219. [[CrossRef](#)]
34. Kunduraci, M.; Amatucci, G.G. Effect of oxygen non-stoichiometry and temperature on cation ordering in  $\text{LiMn}_{2-x}\text{Ni}_x\text{O}_4$  ( $0.50 \geq x \geq 0.36$ ) spinels. *J. Power Sources* **2007**, *165*, 359–367. [[CrossRef](#)]
35. Markovsky, B.; Talyossef, Y.; Salitra, G.; Aurbach, D.; Kim, H.J.; Choi, S. Cycling and storage performance at elevated temperatures of  $\text{LiNi}_{0.5}\text{Mn}_{1.5}\text{O}_4$  positive electrodes for advanced 5 V Li-ion batteries. *Electrochem. Commun.* **2004**, *6*, 821–826. [[CrossRef](#)]
36. Zhong, Q.; Bonakdarpour, A.; Zhang, M.; Gao, Y.; Dahn, J.R. Synthesis and electrochemistry of  $\text{LiNi}_x\text{Mn}_{2-x}\text{O}_4$ . *J. Electrochem. Soc.* **1997**, *144*, 205–213. [[CrossRef](#)]
37. Feng, C.Q.; Li, H.; Zhang, C.F.; Guo, Z.P. Synthesis and electrochemical properties of non-stoichiometric Li-Mn-spinel ( $\text{Li}_{1.02}\text{M}_x\text{Mn}_{1.95}\text{O}_{4-y}\text{F}_y$ ) for lithium ion battery application. *Electrochim. Acta* **2012**, *61*, 87–93. [[CrossRef](#)]



© 2017 by the authors. Licensee MDPI, Basel, Switzerland. This article is an open access article distributed under the terms and conditions of the Creative Commons Attribution (CC BY) license (<http://creativecommons.org/licenses/by/4.0/>).